Analysis of trace impurities in palladium metal powders by glow discharge mass spectrometry

ARTICLE *in* JOURNAL OF ANALYTICAL ATOMIC SPECTROMETRY · SEPTEMBER 1996

Impact Factor: 3.47 · DOI: 10.1039/JA9961100861

3 AUTHORS, INCLUDING:

David Matthew Wayne
Los Alamos National Laboratory
45 PUBLICATIONS **1,122** CITATIONS

JAAS
Journal of Analytical Atomic Spectrometry

Analysis of Trace Impurities in Palladium Metal Powders by Glow Discharge Mass Spectrometry*

DAVID M. WAYNE, THOMAS M. YOSHIDA AND DONALD E. VANCE

Chemical Sciences and Technology Division, Mail Stop G740, Los Alamos National Laboratory, Los Alamos, NM 87545, USA

Metals are often analysed for trace impurities using a combination of techniques (*i.e.*, ICP-MS, ICP-AES, combustion, *etc.*) which offer accurate and precise results for some elements, but not for others. High-resolution glow discharge mass spectrometry (GDMS) offers nearly complete coverage of the periodic table, thus avoiding the necessity of combining results from several techniques to quantitate a wide range of elements in a single sample. GDMS is a direct solids analytical technique, which provides an additional advantage as samples do not have to be dissolved prior to analysis. However, the application of GDMS to the analysis of many important materials, notably the noble metals, is hampered somewhat by a lack of standard reference materials. Reliable standards can be fabricated in-house, but these lack the necessary tracking and certification. The analysis of powdered metals provides additional challenges due to the presence of surface-adsorbed species (H_2O, CO_2, *etc.*), occluded atmospheric gases, and the remnants of chemical processing. However, GDMS analysis of Pd powders for a wide range of trace impurities (C, Al, Si, Fe, Ni, Cu, Zn, Rh, Ag, Cd, Ir, Pt, Au and Pb) provided comparable results to analyses of the same materials by combustion (C), ICP-AES (Si, Fe) and quadrupole ICP-MS (Al, Ni, Cu, Zn, Rh, Ag, Cd, Ir, Pt, Au and Pb).

Keywords: *Glow discharge mass spectrometry; inductively coupled plasma mass spectrometry; combustion analysis; palladium; carbon; relative sensitivity factor*

Glow discharge mass spectrometry (GDMS) presents an appealing alternative to the more established methods for metals analysis, such as ICP-MS, various types of AES and AAS, for several reasons. Many traditional methods require sample dissolution followed, in some cases, by sequential dilution or column separations. Trace analyses of solutions by AAS and AES may be complicated by signal suppression at high analyte concentrations, and by spectral interference from matrix elements. In the case of ICP-MS, analyte signals may also suffer interference and reduced abundance sensitivity due to a variety of metal hydride $[MeH]^+$, metal oxide $[MeO]^+$, metal argide $[MeAr]^+$, and other metal adduct peaks. Determinations of certain light elements, such as carbon and sulfur, by ICP-AES and ICP-MS are precluded entirely due to extensive ionic interferences, and by the unavoidable contamination of sample solutions by dissolved gases (*e.g.*, N_2, CO_2). The implementation of high-resolution, doubly-focusing, magnetic sector mass spectrometers can remedy many, but not all, of these analytical difficulties.

GDMS is a direct analytical technique, whereby the dissolution step and the need for dilution and extraction can be eliminated entirely. Glow discharge sources, both dc- and rf–powered, are very versatile and can be interfaced to a variety of analytical instruments, including AES,[1–4] quadrupole MS[1,5–7] and doubly-focusing sector MS[1,8,9] instruments, among others. Unlike many other direct sampling techniques (*e.g.*, laser ablation ICP-MS), GDMS exhibits relatively uniform elemental response, and can rapidly produce quantitative (or semi-quantitative) trace and ultra-trace (low ppb) analyses of conducting materials without the need for strictly matrix-matched standards. The physical separation of atomization and ionization processes reduces matrix dependence relative to other sputter atomization techniques such as SIMS.[10]

As in ICP-MS, there are numerous interferences in a typical GDMS spectrum. Most of the interfering peaks in a GDMS spectrum are multiply-charged species (absent from most ICP-MS spectra) and metal argides. Unlike ICP-MS, solvent- and atmospheric-derived peaks are much lower, or absent entirely.[11] Small amounts of water vapour, carbon, oxygen and nitrogen occur as contaminants in the GDMS source, and on the sample surface. Samples free of adsorbed H_2O, CO_2 and various hydrocarbons are preferable for GDMS analysis for several reasons: (*i*) the presence of H^+ and O^+ ions in the source produces an unstable discharge, thereby reducing the precision and accuracy of the analyses,[12–15] (*ii*) various carbide, oxide and hydride species may overlap peaks of interest, and (*iii*) meaningful analysis of C contents would be impossible due to the dissociation and ionization of adsorbed organic C and CO_2. The presence of gaseous contaminants in the GDMS source is minimized in a number of different ways: (*i*) by baking-out the source and the sample *in vacuo*, (*ii*) by cryo-pumping the source region, thereby eliminating hydrocarbon mists generated by mechanical pumps, and (*iii*) by cryogenic (*i.e.*, using liquid N_2) cooling of the source.[12,13]

The analysis of metal powders, however, presents additional challenges not normally associated with the analysis of bulk metals by GDMS. For example, oxygen, nitrogen, fluorine, chlorine, sodium, potassium, and water vapour are common contaminants in metal powders, either as thin surface coatings, surface-adsorbed species, or as remnants of a metal powder preparation process (*i.e.*, precipitation from a metal nitrate or chloride solution). For typical bulk metal samples, oxidation coatings and other surface contaminants can easily be sputter-cleaned from the analytical surface. By contrast, metal powders have an exceptionally high number of surfaces, and hence large net surface areas. Thus, contaminant species are present throughout a typical pressed powder sample. Storage in a drying oven may actually exacerbate surface contamination by enhancing the gettering action of certain metals. Additional contamination may be acquired during sample preparation. Metal powders are typically pressed into pellets prior to GDMS analysis. The powder-pressing technique tends to trap ambient gaseous species in pore spaces within the sample. In the GDMS source, occluded gases may either diffuse out of the sample, or are released as the surrounding material is sputtered away.

Palladium is particularly well known for its ability to entrain molecular H_2 within its structure.[16] Mass spectra from a solid Pd sample which was electrolytically charged with H_2O and D_2O showed persistent $[PdH]^+$ and $[PdD]^+$ peaks at m/z

* Presented at the 1996 Winter Conference on Plasma Spectrochemistry, Fort Lauderdale, FL, USA, January 8–13, 1996.

103, 107, 109, 111, 112, 113 and 114 in a cryogenically-cooled source.[17] Hydride and deuteride adducts disappeared from the spectra only after the Pd sample was heated to 800 °C for 1 h in air.[17]

Another stumbling block to the quantification of trace elements (especially halogens, alkali metals and alkaline earths) in metal powders by GDMS is the lack of appropriate certified standard reference materials.[18] Three approaches may be taken to remedy this situation: solid metal Standard Reference Materials (*e.g.*, NIST SRM 1264) can be used as surrogates, a well-characterized metal powder can be used as a standard,[18] or known quantities of high-purity metal powders may be introduced as dopants in an appropriate high-purity metal powder and mixed to yield a 'homemade' standard material. The latter two approaches were applied with great success to the GDMS analysis of platinum powders by van Straaten *et al.*,[18] among others.

At Los Alamos National Laboratory, the quantification of trace carbon in metal powders is traditionally accomplished by combustion techniques.[19] Since GDMS, ICP-AES and ICP-MS were already being applied to determine the concentrations of trace metals in palladium powders, we decided to also measure the total carbon concentrations in the Pd powders using GDMS and compare the results with those obtained by the combustion analyses. An advantage of GDMS analysis is that a wide range of other metallic and non-metallic impurities, in addition to carbon, can be quantified simultaneously and without resorting to a combination of analytical techniques.

INSTRUMENTATION AND PROCEDURES

Combustion Analyses

Combustion analyses for C content in the Pd powders were conducted using an apparatus fabricated in-house. Approximately 50 mg of sample was sealed in a high-purity Sn capsule, which was dropped into a furnace at 1200 °C. The C measurement commenced as soon as the capsule melted (232 °C) and the sample was exposed to an oxygen stream, which converted C to CO_2. The net amount of liberated CO_2 was determined by an IR technique, and was reported as the sum of total inorganic C and total organic C (TIC–TOC) in ppm by mass relative to that of the starting material (minus the Sn capsule blank). The combustion analyses are routinely performed in duplicate. Further details on C determinations in metals *via* combustion are published elsewhere.[19]

ICP-MS and ICP-AES

Multielement analyses were performed using an ARL 3580 ICP-AES (Fisons Instruments, Danvers, MA, USA) for Fe, Mg, Ca, Si, P, K and Na. All other elements were analysed using a Fisons Plasma Quad 2+ ICP-MS. All ICP-MS analyses were run in fully quantitative scanning mode (*i.e.*, a standard for each analyte) using NIST-traceable standards. Internal standards used for ICP-MS were Sc^{45}, Nb^{93}, Tb^{159}, Ho^{165} and Th^{232}. There was little suppression (<10%) of the internal standard signals due to the Pd matrix. In spite of the limited matrix affects, referencing the analyte correction to the nearest (mass) internal standard produced significantly better results than interpolating between multiple internal standards.

A small quantity (0.25 g) of Pd powder was dissolved in 5 ml of fresh *aqua regia* at room temperature for 1 h. This solution was diluted to 25 ml with doubly-deionized water (DDW) in a calibrated flask. Duplicate samples were dissolved using a closed-vessel microwave oven. For the microwave dissolutions, 0.25 g of Pd powder was digested in 5 ml of *aqua regia* in the Teflon vessel liner at room temperature for 1 h. Then, 5 ml of DDW was added, the vessel was capped, and the mixture was heated in a CEM MDS-2000 microwave oven (CEMCORP, Matthews, NC, USA) for 15 min at 84 °C. The vessel was cooled and vented and heated again to 180 °C and 972 kPa, for 15 min. After dissolution the solution was transferred to a 25 ml calibrated flask and made up to volume with DDW.

Table 1 Detection limits for ICP-MS, ICP-AES and GDMS

	Detection limit (ppm)	
Isotope	GDMS	ICP-MS
C^{12}	9	–
Al^{27}	20	1
Si^{28}	3	20*
S^{32}	0.2	–
Fe^{56}	4.1	10*
Ni^{60}	4.5	4.3
Cu^{63}	0.3	–
Cu^{65}	0.3	0.7
Zn^{66}	0.6	3.0
Rh^{103}	0.04	0.1
Ag^{107}	1	0.2
Ag^{109}	1	–
Cd^{114}	0.35	0.1
Cd^{112}	0.35	–
Cd^{113}	0.35	–
Ir^{193}	0.1	–
Ir^{191}	0.2	–
Pt^{195}	0.3	0.1
Pt^{194}	0.3	–
Pt^{196}	0.3	–
Au^{197}	0.7	4.0
Pb^{208}	0.02	0.6

* Denotes detection limit for ICP-AES.

ICP-MS analyses were performed at a minimum dilution of 1:100, while the dilution factor for the ICP-AES was 1:10. The high Pd matrix (~0.1% at a dilution of 1:10) caused few problems for either technique. A 0.1% Pd matrix blank showed no significant background inferences for the ICP-AES analyses. However, a number of isobaric interferences caused difficulties for certain elements in the ICP-MS analyses. In particular, the limited resolution of the quadrupole mass filter may limit the quantification of Rh^{103}, Ag^{107} and Ag^{109} due to reduced abundance sensitivity caused by the presence of the adjacent large Pd peaks (Pd^{104}, Pd^{108} and Pd^{110}).

Detection limits for ICP-MS, ICP-AES (both taking the dilution factor into account) and GDMS are shown in Table 1. The detection limits were estimated as 3 times the standard deviation (3σ) of repeat analyses of the analytical blank (high-purity HNO_3 for ICP; 99.9985% Pd powder for GDMS).

Glow Discharge Mass Spectrometry

Instrumentation

All measurements were performed on a Kratos (Ramsey, NJ, USA) 'Concept' high-resolution, doubly-focusing, dc GDMS. A similar instrument has been described previously.[9] The Kratos GDMS was interfaced to a Sun Sparc Station (Sun Microsystems, Mountain View, CA, USA) which performed data acquisition, mass calibration, *etc.* Raw data (as peak areas) from the Sun Sparc Station were converted to elemental concentrations using a commercially available spreadsheet program (Lotus 1-2-3, version 3.01).

A schematic drawing of the discharge cell for the Kratos instrument (Fig. 1) provides an interesting comparison to the well-characterized VG9000 ion source.[5,12,18,20–22] One important difference between the 'standard' VG9000 ion source and the Kratos ion source (Fig. 1) is that the gap between the sample (cathode) and the Ta anode is much wider in the VG source.[20,21] Although the flat sample configuration is shown in Fig. 1, the Kratos discharge cell can also accommodate

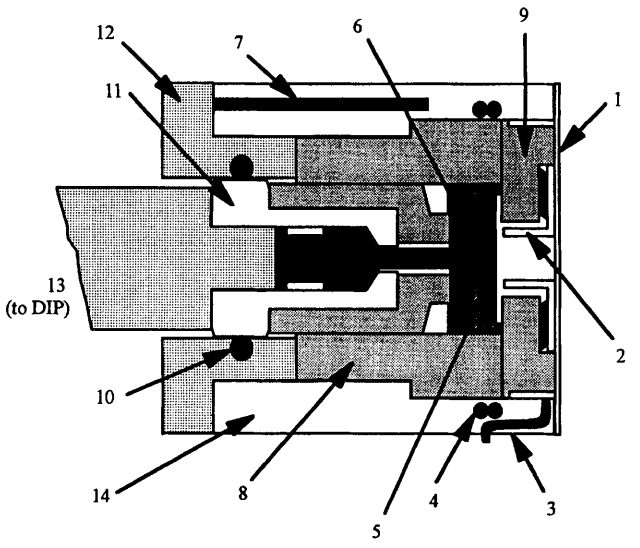

Fig. 1 Schematic drawing (not to scale) of the Kratos glow discharge cell: 1, ion exit plate (Ta or steel); 2, Ta anode; 3, gas inlet; 4, heating coils; 5, flat sample (cathode); 6, sample holder W/clip; 7, thermocouple; 8, inner source insulator (quartz); 9, anode insulator (quartz); 10, electrical contacts; 11 sample mounting device (steel); 12, outer source insulator (Macor or h-BN); 13, insertion probe insulator (Macor); 14, discharge cell housing (steel); and 15, probe tip insulator (quartz).

pin-shaped samples. Further details on sputtering, atomization and ionization processes in the GDMS source are provided in numerous recent publications.[1,10,22,23]

Between samples, the quartz insulators, the Ta anode, and the ion exit plate (either Ta or stainless steel) from the GDMS source were cleaned in warm, concentrated HNO_3, repeatedly rinsed and sonicated in 18 $m\Omega^{-1}\,cm^{-1}$ Milli-Q H_2O and acetone, and oven dried. The carrier gas (99.9999% Ar, US Bureau of Mines) was passed through a heated getter system and into the GDMS source *via* a flexible fused-silica capillary tube. Gas flow was regulated with a needle valve. The source vacuum was maintained by cryopumping. The analyser and detector regions were pumped by three turbopumps which maintained a pressure of less than $\sim 4 \times 10^{-7}$ mPa during operation.

The Kratos GDMS operates routinely at a mass resolution ($M/\Delta M$) of 4000 to 5000, and is capable of $M/\Delta M > 10\,000$ (peak width defined at 10% of peak height). The detection system consists of a Faraday cup detector and a post-acceleration detector (PAD) which can be operated in analogue mode or in ion counting mode (for the measurement of very small signals). All three detector options can be activated during a single scan, thereby enabling the near-simultaneous measurement of matrix ions using the Faraday cup and trace constituents using the PAD in ion-counting mode.

GDMS sample preparation

The Pd samples analysed for this study were ultrafine powders ('Pd black') obtained from several different suppliers. Scanning electron micrographs revealed that individual Pd nodules were spheroidal in shape, and roughly 0.3 to 0.5 mm in diameter. The nodule size of the different Pd powder samples was uniform, except for one (2-17187) which contained a range of nodule sizes from 0.2 to > 2 μm. To provide a basis of comparison for the presence of trace elements in a high-purity Pd powder, several samples of high-purity (99.9985%, Alfa) Pd powder were also analysed. Sample cathodes were prepared by loading approximately 0.5 g of Pd powder into pre-cleaned, disposable Teflon pellet moulds and pressing at 8 kPa for 60 s into a disk 1 cm in diameter by ~0.2 cm thick. The disks were affixed to the sample insertion probe with a disposable steel clip, and introduced into the source. The Kratos 'Concept' GDMS is not equipped with cryogenic (*i.e.*, liquid N_2) source cooling,[12] therefore sample baking *in vacuo* within the GDMS source is necessary to drive off adsorbed H_2O, CO_2 and other surface contaminants. The heating coils used for the source baking were wrapped around the stainless-steel discharge cell housing, just behind the ion exit plate (Fig. 1).

Previous experience in our laboratory indicates that for typical powdered samples (*i.e.*, non-conductors mixed with Ta powder) a 1 h bake-out *in vacuo*, followed by a 30 to 45 min cool-down and 15 to 30 min of pre-sputtering, is sufficient to reduce the H_2O signal from ~1% (relative to Ta^{180}) to < 10 ppm. Significant reductions in the H_2O signal for samples combined with a Ta binder may be attributable to the gettering properties of Ta^+ ions.[24] Although the gettering properties of Pd ions in the glow discharge source (relative to Ta) are not known, mass spectra of all Pd samples analysed for this study, except the high-purity powder (99.9985%, Alfa), contained an unusually large $[H_2O]^+$ peak, despite extensive (up to 16 h) *in vacuo* bakeout at temperatures up to 350 °C. Typical $[H_2O]^+$ signals for the ultrafine Pd powders following bake-out, cool-down and pre-sputtering varied from about 0.2% to about 100 ppm (relative to the total Pd ion current). Extended bake-out, cool-down and pre-sputtering (up to 1 h) did not significantly reduce the $[H_2O]^+$ signal enough to warrant changes in the bake-out procedure. If surface-adsorbed H_2O is driven off by the bake-out procedure, it is possible that structurally-incorporated H_2 (*i.e.*, within the Pd metal particles) is liberated during sputtering, and forms $[H_2O]^+$ *via* interactions with O ions or $[ArO]^+$ clusters in the negative glow region.

GDMS analytical procedure

Prior to analysis, the distance of the sample surface from the anode was set at an optimal distance of ~1.5 mm, although plasma-etching was performed at a slightly larger sample–anode gap to obtain a larger sputtering diameter. Most of the samples were run at a potential of 1.5 kV, with a sample current of 0.5 to 0.8 mA. One suite of samples were run at a potential of 2.5 kV, with a sample current of 0.6 to 1.0 mA in an attempt to produce a more representative analysis by increasing the sputtering rate (thereby consuming more material). Argon pressure in the discharge cell during analysis is not directly measurable, although we estimate it to be 10–100 Pa. During analysis, Ar pressure within the source housing was $\sim 2.63 \times 10^{-3}$ mPa, and the flight tube pressure was $\sim 3.75 \times 10^{-7}$ mPa.

For the first group of analyses (Batch 1), data were obtained by scanning (30 s per decade DAC scan) over a mass range of 5–350 u, using the PAD (post-acceleration detector) in analogue mode. Scanning GDMS data represent the sum of 10 to 15 scans. Duplicate pellets were analysed for two samples, and the reverse side of one pellet was analysed to check homogeneity.

Analyses of another batch of Pd samples were conducted using the 'single-ion monitoring' (SIM) analysis option (Batches 2 and 3), which permitted the use of the PAD in ion counting mode. SIM analyses are analogous to data collected by peak hopping, wherein a very small (in this case, about 0.08 amu) pre-selected portion of the mass spectrum is scanned repeatedly (10 times) for 1 to 3 s. For the Batch 2 analyses, the Pd^{106} peak was set to 10 V at a detector gain of $\sim 5 \times 10^4$ and all analyses were conducted at a detector gain of 1.3×10^6 (equivalent Pd^{106} ~260 V). All Pd isotopes (except Pd^{102}) were monitored on the Faraday cup, and carbon was monitored using the PAD in analogue mode. For the Batch 3 analyses, the Pd^{106} peak was set at 10 V at a gain of $\sim 1.4 \times 10^4$ and all

analyses were conducted at a gain of $\sim 5.2 \times 10^5$ (equivalent Pd^{106} ~ 370 V).

GDMS quantification

For calibration purposes, relative sensitivity factors (*RSFs*) were utilized. RSFs are defined as:

$$RSF_{(x/S)} = (C_x/C_S)/(I_x/I_S) \quad (1)$$

where C and I refer to concentration and peak intensity, respectively, and the subscripts x and S refer to the analyte of interest and an internal standard, respectively. RSFs used in this study are presented in Table 2, along with the results of the linear regressions for the Batch 3 calibrations. For Batch 1, single-point RSFs were determined using repeat analyses of a mixture (of known concentration) of high-purity Pd and Al powders. For the Batch 2 analyses, the C_{Pd}, Al_{Pd} and Si_{Pd} RSFs were acquired *via* repeat analyses of a pellet made of high-purity Pd doped with known weights of C, Al and Si. The Al_{Pd} RSF (*i.e.*, the RSF for Al in a Pd matrix) was used, in both instances, to calculate the remaining RSFs from repeat analyses of NIST SRMs 500 (Unalloyed Copper–Cu VII), 1250 (High Temperature Alloy Fe–Ni–Co) and 1259 (Aluminum Alloy 7075). Agreement for RSFs acquired using different standards was 11% relative (2σ). For Batch 2 analyses, the following elements were quantified in addition to Pd and C: Al, Si, S, Fe, Ni, Cu, Rh, Ag, Pt, Au and Pb, although RSFs were not obtained for Rh, Pt and Au.

For the Batch 3 analyses, high-purity powders of several different elements (C, Al, Si, Fe, Ni, Pd, Ag, Pt) and oxides (CuO, IrO_2) were carefully weighed and mixed for 15 s in a pre-cleaned polycarbonate vial using a Wig-L-Bug powder homogenizer. The homogenized powder was then dispersed in Ta powder (99.9985%, Alfa) and sequentially diluted to yield three different abundance levels for each element. Each of these Ta-powder standards were pressed into pellets and analysed by GDMS as described above. To check for homogenous mixing in the 'standard' pellets, one of the three standards was analysed on both sides (front and back). Ion beam ratios for each isotope of each element were then plotted against the mass abundance–normalized concentration ratio relative to Ta and linearly regressed. The slopes of these lines are equivalent to the RSF of each element relative to Ta. RSFs relative to Pd were then calculated by normalizing to the Pd_{Ta} RSF (Table 2). A similar technique was used to determine both the Rh_{Ta} *RSF* by using a 1% Rh on Al_2O_3 material (Alfa–Johnson-Matthey) and the Pb_{Ta} RSF using Pb_3O_4 powder (99%, Aldrich). The RSFs for Al, Pd, and Pt (relative to Ta) determined two months earlier by the same technique are very similar to those used for Batch 3 (Table 2). The *RSF* for Au (relative to Pd) was determined using a powdered Pt_{40}–Au_{40}–Pd_{20} alloy (99.9%, Alfa). The Zn_{Pd} RSF was estimated from repeat measurements of the Cu_{Al} and Zn_{Al} RSFs in NIST SRMs 1259 and 1256a, and applying the resulting Zn_{Al}:Cu_{Al} ratio (0.9) to give an estimate of the Zn_{Pd} RSF from the Cu_{Pd} *RSF*. The S_{Pd} RSF was estimated by normalizing the S_{Fe} *RSF* measured in NIST SRM 663 to the Fe_{Pd} RSF.

Table 2 Relative sensitivity factors ($RSF_x = b_x$), for GDMS analyses of Pd. For Batch 3, calibration parameters (a_x), goodness-of-fit parameters (R), and number of measurements (n) of impurity elements in Ta and Pd are listed. Standard deviations (in parentheses) are quoted at 2σ uncertainty, values are given in parentheses

Element	Batch 2 RSF_{Pd}	Batch 3 RSF_{Ta}	a_{Ta}	R	n	RSF_{Pd}
C	0.54	1.33(3)	−0.00002(2)	0.995	29	1.41
S	0.56					0.73†
Al	0.77	0.58(2)	0.0003(8)	0.993	13	0.62
Al*		0.56(2)	−0.0002(4)	0.989	32	
Si	1.02	0.92(1)	-6.32×10^{-6}	0.996	36	0.98
Fe	0.78	0.809(8)	−0.00001(9)	0.999	17	0.86
Ni	1.11	1.04(1)	−0.00003(4)	0.995	55	1.11
Cu	2.44	1.61(4)	−0.00002(11)	0.993	24	1.71
Rh	ND‡	1.06(1)	1.95×10^{-6}	0.999	19	1.13
Pd	1	0.94(1)	−0.00002(2)	0.996	66	1
Pd*		0.96(1)	−0.00002(6)	0.999	41	
Ag	1.46	0.95(2)	0.00042(8)	0.997	22	1.01
Ir	NA	0.67(1)	0.00007(5)	0.997	23	0.71
Pt	ND	1.004(7)	0.00005(3)	0.999	65	1.07
Pt*		1.05(1)	0.0010(2)	0.999	41	
Au	ND				6	1.50
Pb	1.59	0.68 (6)			18	0.73
Zn						1.54†

* Previous determination.
† Estimated value.
‡ ND—not determined.
§ NA—not analysed.

RESULTS AND DISCUSSION

Carbon

All C concentrations determined by GDMS and by combustion methods are shown in Fig. 2. Carbon data from GDMS analyses (SIM only) are also shown in Table 3. Carbon concentrations are typically <200 ppm in the Pd powders. The highest C contents (>400 ppm) were observed in samples (*e.g.*, S2-REF, Fig. 2A) prior to bake-out. Following bake-out, the C level in the same samples was 130 to 140 ppm. A high-purity (99.9985%, Alfa) Pd sample (Fig. 2B) showed higher C contents prior to bake-out (40 ppm) than after (26 ppm). The relative precision (1σ) of total C measurements by GDMS was similar for both internal (3 to 22%) and external duplicates (4 to 17%) duplicates when analysed in scanning mode. For the same samples, the precision of duplicate analyses by the combustion technique varied from 2 to 45% relative (1σ). For C, SIM analyses (Fig. 2B) proved to be somewhat less precise (6 to 37%) than the scanning analyses, and were much less precise than the combustion analyses (0 to 8%).

Most of the C analyses obtained by GDMS compare marginally well with those obtained using combustion techniques. With the exception of four samples (S2-CF, 2-6FT, 2-4FP and S2-RECD), the scanning mode GDMS results (Fig. 2A) are between −38 and +42% of the combustion analyses. When potentially contaminated samples (2-17263 and high-purity Pd, Fig. 2B) are ruled out, agreement between SIM-mode GDMS and combustion analyses was consistently better (−30 to +25%) than shown by the scanning-mode analyses.

Two factors may account for the apparent lack of precision in the analysis of C in the Pd powders by GDMS: (*i*) the possibility of contamination and (*ii*) the likelihood of sample heterogeneity on the μg scale. Carbon is ubiquitous, and contamination from a variety of sources (Teflon pellet moulds, clothing fibres, particulate organic matter, *etc.*) could have been introduced into some of the samples, despite careful sample preparation practices. For example, the high-purity Pd powder may have been contaminated with a carbon-rich substance prior to preparation of the pellet for the final analysis (Fig. 2B).

Analytical volume is an important consideration for the direct analysis of heterogeneously distributed trace elements in solids.[25] Combustion analyses consumed 50 mg of Pd sample per analysis. The actual sample size for a GDMS analysis can be estimated by measuring the total weight loss of several pellets before and after analysis. The average weight loss of three samples after ~ 3 h of sputtering was 19 ± 1 mg, which corresponds to a sputter rate of ~ 0.11 mg min^{-1}. Each SIM analysis lasted 30 min, thus the amount of Pd removed during

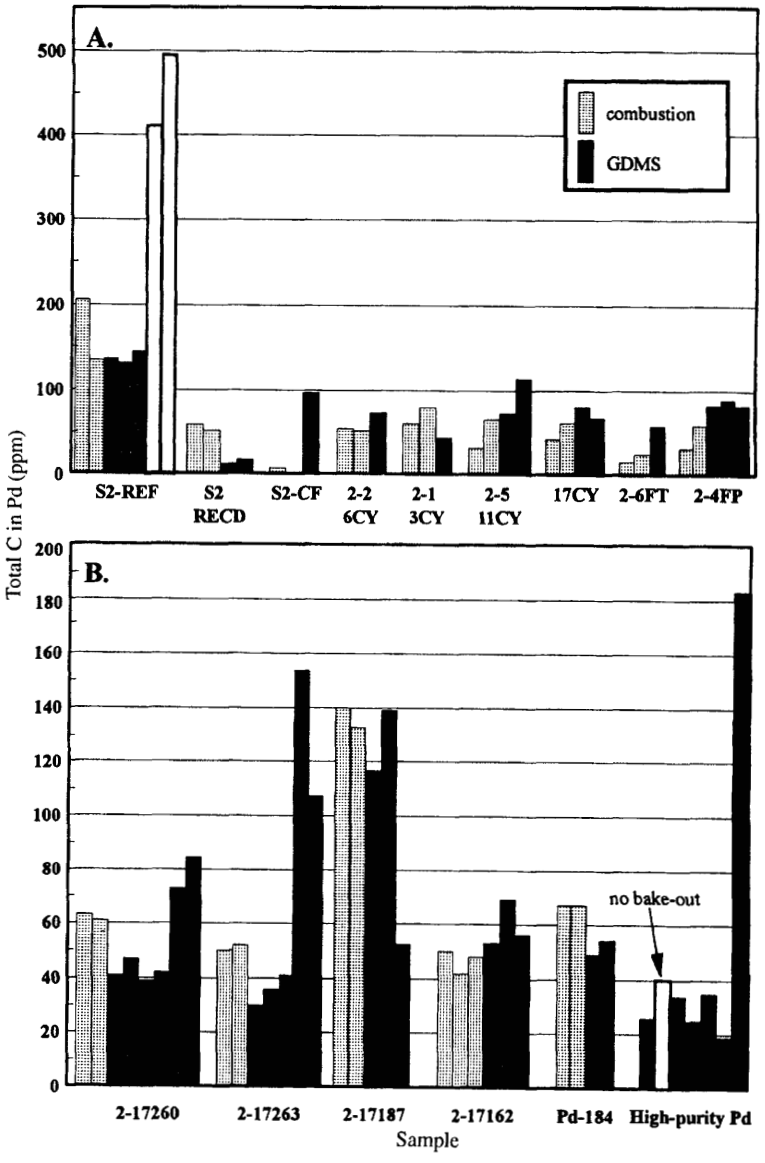

Fig. 2 Carbon contents in Pd powders determined by combustion techniques (light stipple) and GDMS (heavy stipple). Samples analysed by GDMS prior to the bake-out step are represented by unshaded bars. A, GDMS data collected in scanning mode (Batch 1); B, GDMS data collected in single-ion monitoring (SIM) mode (Batches 2 and 3). Anomalously high C values in two samples 'High-purity Pd' and '2-17263') may represent contamination.

a single analysis is, at most, ~3.5 mg. Therefore, the analytical volume for the GDMS is over an order of magnitude lower than for combustion. One-dimensional heterogeneities in trace element content at this scale are observable *via* depth profiles of the Pd powder pellets (Fig. 3), which indicate that C impurities are heterogeneously distributed relative to the trace metals (*e.g.*, Rh) in at least two of the samples.

Other Trace Constituents

Spectral interferences

Even with the high resolving capability of the magnetic sector GDMS, Al, Cr and Mn peaks suffered from lowered abundance sensitivity. Persistent, broad interference peaks (*e.g.*, Fig. 4) overlap Al^{27}, Cr^{52}, Cr^{53}, and Mn^{55} and result in abnormally high backgrounds (~20 to 50 ppm) for these analytes. High backgrounds were also present in the vicinity of the Fe^{56} and Ni^{60} peaks, but the analyte peaks were much more intense than the background. In the case of Mn and Cr (Fig. 4), the high background may be due, in part, to the superimposition of interference peaks from a combination of sources: Ar adducts (*e.g.*, $[Ar^{40}C^{12}]^+$, $[Ar^{36}O^{16}]^+$, $[Ar^{38}N^{14}]^+$) and doubly-charged Pd ions (*e.g.*, $[Pd^{104}]^{2+}$, $[Pd^{106}]^{2+}$, and $[Pd^{110}]^{2+}$). The Cr, Mn and Ni background was significantly reduced (to <1 ppm) when steel slits were replaced with Ta slits following the completion of the Pd analyses. The origin of the high background in the vicinity of the Al peak is not known, as the most likely isobars (*e.g.*, $[C_2H_3]^+$, HCN^+, $[Fe^{54}]^+$, *etc.*) are easily resolvable at the operating resolution of 4000.

Interference at *m/z* 197 was greatly enhanced only during the Batch 2 analyses, which were performed at a 2.5 kV sputtering potential. We observed significant increases (*i.e.*, from background levels) in the intensity of broad peaks at *m/z* 197 ($[TaO]^+$) and *m/z* 181 (Ta^+) as the sputtering potential was increased from 1.5 to 2.5 kV at a constant Ar pressure and sample-anode gap. The very close proximity of the sample surface to the cathode (Fig. 1) suggests that the origin of the Ta^+ and $[TaO]^+$ peaks may be Ta sputtered from the surface of the anode. Oxygen, also present in the Pd samples, reacts readily with Ta^+ ions in the GDMS source to form $[TaO]^+$ ions[24], which are not resolvable from Au^+ at the operating resolution of 4000 to 5000.

For the quadrupole ICP-MS analyses, scans of a 0.01%

Table 3 GDMS, ICP-MS and ICP-AES (Si and Fe only) analyses of Pd powders. Results quoted in ppm. Standard deviations (in parentheses) quoted at 1σ uncertainty

Element	Batch 3* Pd-184 ($n=4$)	Batch 3 Pd-184 ($n=4$)	Batch 3 2-17187 ($n=4$)	Batch 2 2-17187 ($n=2$)	ICP-MS	Batch 3 2-17260 ($n=4$)	Batch 3 2-17260 ($n=4$)	Batch 2 2-17260 ($n=4$)	ICP-MS
C^{12}	49 (3)	55 (6)	50 (9)	128 (11)	NA	72 (6)	86 (6)	42 (3)	NA
C^{13}	44 (4)	57 (9)	45 (10)	NA		65 (6)	72 (10)	NA	
A^{127}	<20	<20	<20	40 (8)	4.3	<20	<20	<20	5.5
Si^{28}	21 (3)	29 (11)	28 (5)	37 (3)	<20	17 (3)	27 (2)	20 (4)	<20
S^{32}	20 (3)	26 (2)	2.2 (0.4)	3.5 (0.7)	NA	1.33 (0.05)	1.4 (0.2)	1.5 (0.2)	NA
Fe^{56}	190 (4)	152 (9)	183 (15)	88 (3)	58	64 (2)	86 (30)	52 (4)	29
Fe^{57}	NA‡	148 (13)	NA	NA		NA	70 (8)	NA	
Ni^{60}	120 (25)	48 (1)	57 (5)	9 (2)	<4.3	82 (4)	82 (3)	16.8 (0.7)	<4.3
Ni^{62}	104 (23)	40 (2)	46 (4)	NA		72 (2)	81 (12)	NA	
Cu^{63}	8.2 (0.3)	8.6 (0.4)	66 (5)	75 (5)		8.2 (0.2)	7.8	0.5	12.0 (1)
Cu^{65}	8.3 (0.1)	8.6 (0.7)	64 (4)	NA	78	8.2 (0.4)	8.2 (0.9)	NA	8.5
Zn^{66}	NA	24.6	NA	NA	7.9	NA	NA	NA	14
Rh^{103}	12 (1)	11.3 (0.8)	96 (10)	34 (2)	45	34.3 (0.8)	36 (2)	19 (2)	15
Ag^{107}	9 (1)	9 (1)	5.8 (0.6)	8.5 (0.8)	30	25.5 (0.7)	26.0 (0.6)	44 (4)	64
Ag^{106}	9 (1)	9 (1)	5.6 (0.9)	7.0 (1.2)		26 (1)	25 (1)	44 (4)	
Cd^{114}	1.1 (0.4)	0.7 (0.2)	0.8 (0.2)	NA	<0.1	<0.35	0.5 (0.1)	NA	0.2
Cd^{112}	1.8 (1.3)	0.9 (0.3)	0.8 (0.3)	NA		<0.35	0.5 (0.1)	NA	
Cd^{113}	1.2 (0.9)	0.6 (0.2)	0.4 (0.3)	NA		<0.35	<0.35	NA	
Ir^{193}	61 (8)	58 (1)	9.5 (0.5)	NA	NA	0.18 (0.02)	0.22 (0.02)	NA	NA
Ir^{191}	58 (7)	55 (1)	9.4 (0.3)	NA		0.7 (0.03)	0.024 (0.3)	NA	
Pt^{195}	15 (1)	16.4 (0.3)	307 (16)	119 (6)	272	38 (1)	41 (2)	26 (2)	32
Pt^{194}	15 (1)	15.9 (0.4)	304 (16)	117 (5)		38 (1)	41 (3)	22 (2)	
Pt^{196}	15 (2)	16.1 (0.5)	296 (14)	117 (5)		37 (1)	42 (2)	25 (2)	
Au^{197}	NA	2.9 (0.2)	1.9 (0.3)	<200	12	6.6 (0.7)	6.9 (0.5)	<200	17
Pb^{208}	1.4 (0.1)	1.7 (0.1)	0.95 (0.17)	NA	0.61	0.82 (0.07)	0.89 (0.09)	1.9 (0.3)	<0.6
With Pd Hydride correction									
Rh(corrected)	12 (1)	11.3 (0.8)	96 (10)			34.3 (0.8)	36 (2)		
Ag^{107}(corrected)	5.5 (0.9)	5.8 (1.1)	3.0 (0.7)			23 (1)	25.1 (0.5)		
Ag^{109}(corrected)	5.1 (0.5)	5.6 (0.9)	2.7 (0.4)			23 (2)	23.6 (0.8)		

Element	Batch 3 2-17162 ($n=4$)	Batch 2 2-17162 ($n=3$)	ICP-MS	Batch 3 2-17263 ($n=4$)	Batch 3 2-17263 ($n=3$)	Batch 2 2-17263 ($n=3$)	ICP-MS	Batch 3 High purity ($n=4$)	Batch 2 High purity ($n=4$)
C^{12}	58 (9)	52 (15)	NA	154 (39)	107 (6)	35 (4)	NA	183 (32)	22 (3)
C^{13}	55 (12)			NA	NA	NA		183 (44)	NA
A^{127}	<20	<20	3.9	32 (2)	<20	<20	29	15 (7)	12 (5)
Si^{128}	10 (2)	14 (1)	29	5.5 (1.1)	3.4 (0.2)	3.2 (0.4)	NA	31 (1)	8.3 (0.7)
S^{32}	1.05 (0.08)	2.01 (0.06)	NA	0.64 (0.06)	0.73 (0.05)	2.5 (0.5)	NA	0.5 (0.1)	0.47 (0.06)
Fe^{56}	65 (2)	32 (4)	39	30.5 (0.9)	36 (3)	145 (10)	39	34 (1)	34 (9)
Fe^{57}	NA	NA		27.2 (0.9)	29 (2)	NA		27 (5)	NA
Ni^{60}	54 (3)	5.6 (1.1)	<4.3	73 (4)	30 (2)	10.6 (0.9)	<4.3	100 (8)	4.3 (0.7)
Ni^{62}	47 (5)	NA		66 (3)	29 (1)	NA		89 (10)	NA
Cu^{63}	1.65 (0.08)	3.1 (0.7)		9.4 (0.2)	9.2 (0.3)	16 (3)		0.5 (0.4)	0.49 (0.12)
Cu^{65}	1.5 (0.1)	NA	2.6	9.8 (0.6)	9.7 (0.4)	NA	14	0.31 (0.09)	NA
Zn^{66}	NA	NA	4	2.8 (0.6)	2.4 (0.3)	NA	39	0.7 (0.2)	NA
Rh^{103}	29 (1)	14 (3)	14	25.9 (0.3)	30.8 (0.6)	14 (2)	15	0.52 (0.01)	1.29 (0.05)
Ag^{107}	5.0 (0.5)	10 (1)	28	102 (19)	93 (5)	115 (29)	47	1.0 (0.4)	7.5 (0.3)
Ag^{109}	4.7 (0.3)	10 (2)		29 (13)	15 (1)	53 (8)		0.8 (0.2)	5.7 (0.3)
Cd^{114}	<0.35	NA	<0.3	0.44 (0.02)	0.38 (0.05)	NA	0.7	1.2 (0.6)	NA
Cd^{112}	<0.35	NA		35 (3)	37 (2)	NA		2.3 (0.2)	NA
Cd^{113}	<0.35	NA		3.2 (0.8)	1.86 (0.06)	NA		0.31 (0.05)	NA
Ir^{193}	0.41 (0.02)	NA	NA	0.9 (0.2)	1.14 (0.08)	NA		1.51 (0.04)	NA
Ir^{191}	0.37 (0.06)	NA		0.50 (0.05)	0.64 (<0.01)	NA		1.41 (0.07)	NA
Pt^{195}	25 (1)	13 (3)	22	24.6 (0.3)	33 (2)	18 (4)	28	0.71 (0.09)	2.8 (0.8)
Pt^{194}	25.1 (0.8)	13 (3)		25.1 (0.6)	34 (1)	18 (4)		0.69 (0.09)	0.27 (0.19)
Pt^{196}	25 (1)	13 (2)		26.4 (0.7)	35 (1)	20 (5)		0.85 (0.08)	2.3 (0.7)
Au^{197}	4.8 (2)	<200	18	0.78 (0.02)	1.02 (0.08)	<200	14	2.1 (0.2)	234 (10)
Pb^{208}	3.7 (0.1)	7 (2)	4.4	10.1 (0.3)	13.2 (0.7)	19 (5)	16	0.02 (0.01)	0.62 (0.23)
With Pd Hydride correction									
Rh(corrected)	12 (1)	11.3 (0.8)	96 (10)			34.3 (0.8)	36 (2)		
Ag^{107}(corrected)	5.5 (0.9)	5.8 (1.1)	3.0 (0.7)			23 (1)	25.1 (0.5)		
Ag^{109}(corrected)	5.1 (0.5)	5.6 (0.9)	2.7 (0.4)			23 (2)	23.6 (0.8)		

* Batch 3: Cathode potential = 1.5 kV, sample current = 0.6 to 0.8 mA. Data for Cd are semi-quatitative (no RSF).
† Batch 2: Cathode potential = 2.5 kV, sample current = 0.7 to 1.0 mA. Data for Au, Pt and Rh are semi-quantitative (no RSFs).
‡ NA—not analysed.

NIST Pd standard showed little $[PdH]^+$ formation, but contributions from the matrix signal resulted in overestimation of Rh and Ag concentrations. For the GDMS analyses, it is possible that Rh and Ag peaks contain contributions from isobaric Pd hydrides ($[Pd^{102}H]^+$ at m/z 103, $[Pd^{106}H]^+$ at m/z 107, and $[Pd^{108}H]^+$ at m/z 109). In a GDMS source without cryogenic cooling, ArH^+ clusters form readily from collisions involving Ar^+ ions and H_2O neutrals.[17] Metal

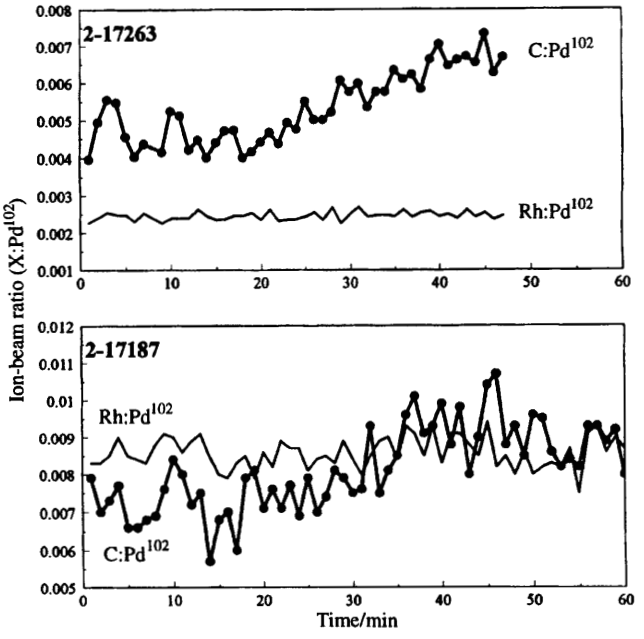

Fig. 3 Depth profile ion-beam ratio data from two compacted Pd powder pellets (2-17263 and 2-17187). For 2-17263, the $C^{12}:Pd^{102}$ ion beam ratio increases through time, relative to the $Rh^{103}:Pd^{102}$ ion beam ratio, which retains a relatively flat profile. In 2-17187, while there is no systematic trend, the variation (1σ) of the $C^{12}:Pd^{102}$ ion beam ratio (13.4%) is much greater than that of the $Rh^{103}:Pd^{102}$ ion-beam ratio (4.8%).

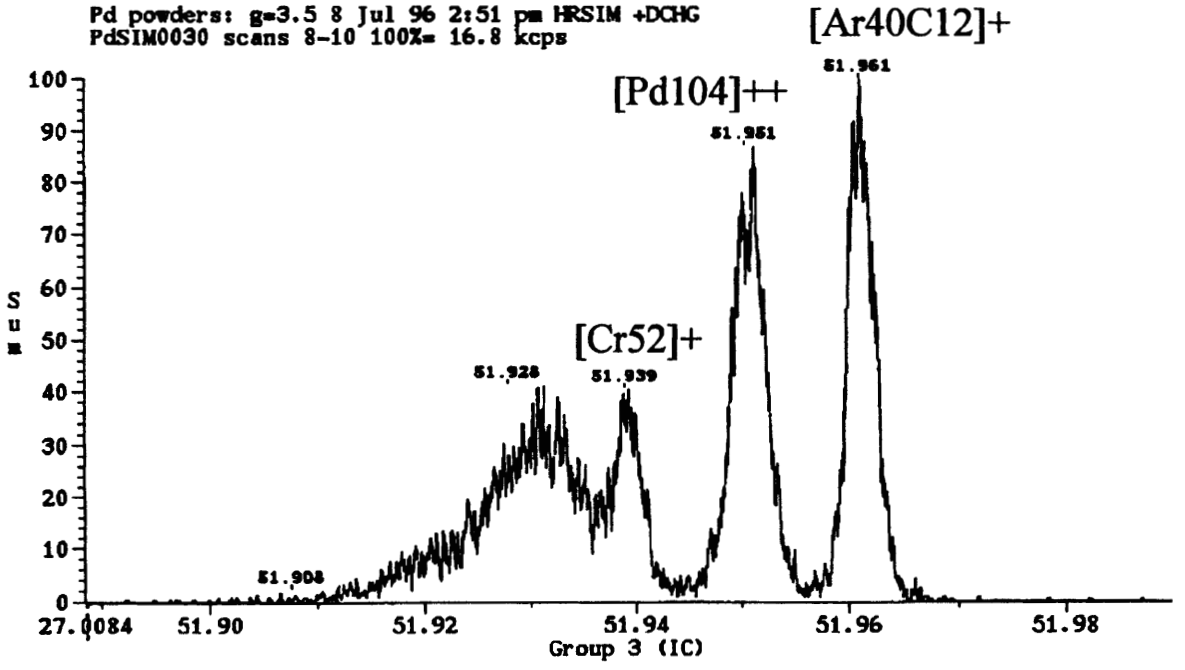

Fig. 4 Typical spectral interferences (an unidentified peak, $[Cr^{52}]^+$, $[Pd^{104}]^{++}$ and $[Ar^{40}C^{12}]^+$) at *m/z* 52 for a Pd powder sample (2-17187). This spectrum was taken at $M/\Delta M \sim 5700$, slightly higher than the normal operating resolution of 4000 to 5000.

hydrides then may be formed in the negative glow region through gas-phase proton exchange between Me^+ and $[ArH^+]$.[17] The persistence of the PdH^+ signals in the GDMS source, even after extended bake-out at 250 °C, is also related to the ability of Pd metal to entrain H_2 within its structure.[16,17] The resolving power required to separate the Pd hydrides from Rh^{103}, Ag^{107} and Ag^{109} ($M/\Delta M = 12{,}975$, 18,013, and 15,524, respectively) is greater than that available using commercial magnetic sector instruments.

Recently, Takahashi and Shimamura[26] developed a simple mathematical model to correct for Fe, Cr, Mn and Ni argide interferences on Zr, Nb and Mo isotopes in steels and meteorites. For this study, their model was adapted to perform a similar calculation to correct for isobaric Pd hydride interferences with Rh and Ag isotopes for the Batch 3 analyses. The calculation of a Pd hydride production ratio at *m/z* 111 was complicated slightly by the presence of sub-ppm quantities of Cd in the Pd samples (Table 3). Several Cd peaks were monitored (Cd^{111}, Cd^{112}, Cd^{113}, Cd^{114}), and the Cd^{111} peak was clearly enhanced relative to the others. A plot of the ion beam ratios (relative to the Pd^{110} peak) of *m/z* 111 (*i.e.*, the combined Cd^{111} and $[Pd^{110}H]^+$ signals) and at *m/z* 113 (*i.e.*, Cd^{113}, which has nearly the same isotopic abundance as Cd^{111}) *versus* the (H_2O:total Pd) ion beam ratio (Fig. 5) suggests that there is an anomalous enhancement of the peak at *m/z* 111. Although the enhanced signal at *m/z* 111 probably represents the contribution of $[Pd^{110}H]^+$, more work needs to be done to determine the exact relationship between the H_2O

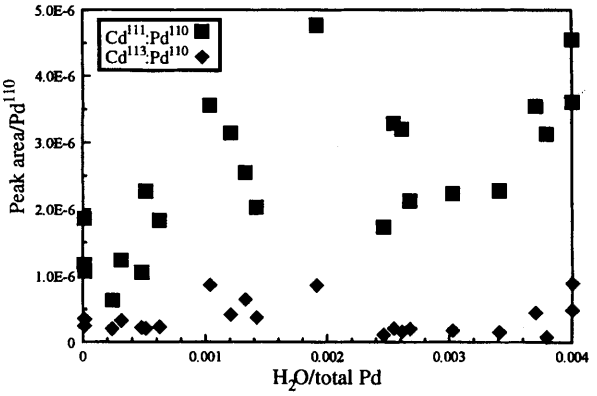

Fig. 5 Comparison of ion beam ratios (relative to Pd^{110}) for m/z 111 (*i.e.*, $[Pd^{110}H]^+$ and $[Cd^{111}]^+$) and m/z 113 (*i.e.*, $[Cd^{113}]^+$ only). The peak intensity at m/z 111 is clearly enhanced over m/z 113, indicating the presence of some $[PdH]^+$ in the discharge. The slight difference in the isotopic abundances of Cd^{111} (12.75%) and Cd^{113} (12.26%) is not sufficient to account for the observed differences in peak intensities.

peak intensity and the intensities of the attendant metal hydride peaks.

If we assume that the enhancement of the Cd^{111} peak is a response to the H_2O content of the sample, the hydride correction should be relatively straightforward.[26] The peak area ratio of m/z 111 to Pd^{110} ($[m/z]^{111}:Pd^{110}$) varied from about 1×10^{-6} to about 5×10^{-6} for each analysis, and is significantly greater than the $Cd^{113}:Pd^{110}$ ratio (Fig. 5). The Cd isotopes at m/z 111 and m/z 113 have similar isotopic abundances (12.86 and 12.34%, respectively), so the $Cd^{113}:Pd^{110}$ ratio was used as an approximation of the ideal (*i.e.*, Pd hydride-free) $Cd^{111}:Pd^{110}$ ratio. The difference between the ($[m/z]^{111}:Pd^{110}$) ratio and the $Cd^{113}:Pd^{110}$ ratio, typically a value between 1×10^{-6} and 1×10^{-7}, was assumed to be equal to the hydride production rate at m/z 111 for each Pd analysis.[26] If Pd hydride production ratios at m/z 103, 107 and 109 are similar, the hydride contributions at these mass-to-charge ratios (corrected for mass abundances of the different Pd isotopes) can then be ratioed to the peak intensities of Pd^{102}, Pd^{106} and Pd^{108}, and subtracted from the observed ion beam ratios (*i.e.*, $[m/z]^{103}:Pd^{102}$, $[m/z]^{107}:Pd^{106}$, and $[m/z]^{109}:Pd^{108}$) to yield hydride-corrected ion beam ratios. The hydride correction calculations indicate that contributions of Pd hydride in the GDMS source at m/z 107 and 109 are at the 1 to 4 ppm level, which corresponds to a 10 to 50% reduction of the apparent Ag concentration when the hydride correction is applied (Table 3). Hydride corrections for Rh are negligible due to the low abundance of the Pd^{102} isotope (0.96%) which makes a relatively small (<0.1 ppm) contribution of $[Pd^{102}H]^+$ to the signal at m/z 103.

Comparison of results using GDMS and ICP

For brevity, only the microwave-assisted ICP data and the GDMS data collected in SIM mode are reported in Table 3. These data represent the average of 2 to 4 SIM analyses of each sample, with 1σ standard deviation. Both the ICP and the GDMS results show that all of the Pd samples are relatively pure and free of metallic impurities >300 ppm. Both methods confirm that most of the samples contain trace amounts of Si, S, Fe, Ni, Cu, Rh, Ag, Ir, Pt, and Au (Table 3). Other trace elements (some not shown in Table 3) present in some samples include Al, Cr, As, Sb, W, Mn, Co, Mo, Cd, Sn, Hg, Pb and Tl. For the ICP analyses, there was little difference between the trace element chemistries of samples digested at room temperature and those at high temperature, except for Al, Zn, and Au where microwave-assisted digestion significantly enhanced the analyte signal. The non-microwaved ICP samples also showed elevated levels of vanadium, possibly due to interference from $[ArNH]^+$.

The Batch 2 and Batch 3 GDMS analyses were conducted at different GD potentials, and duplicate analyses of the same samples at different potentials indicate marginal precision (>30% error relative, 1σ) for most trace elements. At 2.5 kV (Batch 2), the presence of a large $[TaO]^+$ peak hindered accurate determination of Au concentrations. Conversely, Ni is 2 to 5 times higher in the Batch 3 (1.5 kV potential) analyses than in the Batch 2 analyses. There is also a 5 to 10% difference in Ni concentrations calculated from the Ni^{60} and the Ni^{62} peak areas, which suggests that the problem may be related to interference from an undetermined source. Agreement (1σ) between GDMS analyses conducted at different GD potentials was somewhat better for Cu (10 to 87%), Si (15 to 42%, excluding 'Spec Pure' Pd) and S (9 to 38%, excluding 2-17162 and 2-17263).

For most trace elements, both internal precision (*e.g.*, standard deviations of individual analyses) and analytical precision (*e.g.*, percentage error for analyses of duplicate samples) improved for analyses conducted at 1.5 kV GD potentials (Batch 3). Figures of merit for Cu, Ag, Rh and Pt are below 10% relative (1σ) for 2 of the 3 'Batch 3' duplicates (Pd 184 and 2-12760), and are below 30% relative for all remaining elements, except Si, Fe and Ni. Precision is somewhat lower for most trace elements in the analyses of the 2-17263 duplicate, but the majority are still lower than 30% relative.

Agreement between GDMS and ICP-MS analyses of the same material is marginal at the ppm level, and is generally better for metals (*e.g.*, Pb, Cu), than for transition elements and light elements (Table 4). Few direct comparisons of GDMS *versus* ICP-MS performance have been published,[11,27,28] and only Teng *et al.*[27] have examined field samples in addition to standard reference materials. The level of agreement between GDMS and ICP-MS analyses of Pd powders demonstrated here is similar, at the ppm level, to that shown by Teng *et al.*[27] for Sr, Ba, and U in soil samples. The level of agreement between GDMS and spark-source ICP-MS[28] at the 100s of ppm level in a steel SRM is far superior for most elements than the results of this study suggest.

Compared with the ICP-AES and ICP-MS results, GDMS analyses show higher concentrations of Al, Si, Fe, and Ni in the Pd powders. For Ni and Fe however, agreement is poor even for duplicate Pd powder samples analysed by GDMS (Table 3). Silver concentrations measured by GDMS and ICP-MS show the same general trends, but the GDMS Ag concentrations are consistently lower than the ICP-MS results for all samples except 2-17263 (Table 4). The disparity between Ag concentrations measured by GDMS and ICP-MS is due to both the contributions of Pd hydride peaks at m/z 107 and 109, and to limited abundance sensitivity of ICP-MS on the low mass side of m/z 104, 108 and 110 due to matrix effects.

One sample, 2-17263, showed anomalously strong peaks at m/z 107, 112, 113, and possibly at m/z 109 when analysed by GDMS. Therefore, the Ag and Cd concentrations measured at these m/z are also anomalous (Table 3), and remained so even after the hydride corrections were applied. The lack of agreement amongst Ag and Cd isotopes indicates that these anomalies are due to ionic interferences, but the interfering species has not yet been identified.

CONCLUSION

Analyses of fine Pd powders for trace amounts of carbon by GDMS compare moderately well with the results of combustion analysis. Unlike carbon analyses in *solid* metal samples by GDMS, which are generally of high quality,[8] the quantification of carbon in the Pd metal *powders* proved, in this case,

Table 4 Ranges (minimum/maximum) in percentage error (relative to the GDMS analysis, 1σ) between GDMS and ICP-MS (or ICP-AES) data for trace elements in Pd powders

Element	2-17187	2-17260	2-17162	2-17263
Al	+81%/+89%	+62%/+79%	+70%/+85%	+9.4%
Fe				−28%/+73%
Cu	−22%	−3%	−76%	−44%/−43%
Zn				< −1300%
Rh*	−31%/+52%	+22%/+59%	−3%/+53%	−7%/+51%
Ag*	< −250%	−150%/−47%	−458%/−171%	+51%/+59%
Cd†				−84%/−59%
Pt	−130/+11%	−23/+21	−66/+12	−56%/+20%
Au‡	−525%	−158%/−146%	−275%	< −1300%
Pb	+52%	+13/+40%	−58%/+16%	

* Not corrected for hydride interferences.
† No RSF.
‡ Batch 3 only.

to be problematic. Additional care in sample handling (*i.e.*, exclusively under Class 100 conditions) and storage may reduce some of the analytical uncertainties observed here. However, it seems likely that sample inhomogeneity at the mg level is an important component of the variability in the GDMS analyses.

GDMS provides data on microsamples (~1 mg), whereas the combustion techniques and ICP-MS provide bulk analyses on 50 to 250 mg samples. Increasing the sputtering rate did not appear to 'smooth out' the trace element contents, possibly because operation at a higher sputtering potential (2.5 kV) resulted in some loss of beam stability. When a representative analysis of a large amount of material is required, a bulk analytical approach such as ICP-MS may take precedence. Conversely, GDMS is a potentially sound method for quantifying *in situ* microscopic variations in elemental concentrations of solid samples.[3,29,30]

Calibration may be a problem when using the GDMS for certain applications simply because high-quality standard reference materials simply do not exist. Certified reference standards for solution-based ICP techniques are abundant, and when these are not available standards can be fabricated in-house by preparing solutions of known concentration from high-purity reagents. However, few (if any) NIST-certified solid standards for trace metals in precious or noble metal matrices (*e.g.*, Pt, Pd, Au, Ag, *etc.*) are currently available. Results from this study, and recent studies by other investigators,[18] suggest that mixed metal powder and oxide powder standards fabricated in-house may provide sufficient accuracy. Even so, there is a great need for certified solid standard reference materials prepared expressly for use with GDMS and allied techniques.

Finally, trace metal analysis by both GDMS and by ICP-MS show that the different Pd samples (often from different suppliers) have distinct trace element signatures. Several elements, most notably Cu, Rh, Ag, Ir, Au, Pt and Pb, showed distinct variations in concentrations between samples. It is possible that these trace element concentrations could be used as a characteristic to label or trace the provenance of high-purity noble metals.

The authors would like to thank David Frost (Kratos), Lorraine Rivera and Chris Brink for their assistance in the laboratory, Tom Zocco for expert SEM work, and E. Larry Callis and Jose Olivares for their comments on an earlier version of this manuscript.

REFERENCES

1 Harrison, W. W., Barshick, C. M., Klingler, J. A., Ratliff, P. H., and Mei, Y., *Anal. Chem.*, 1990, **62**, 943–A.
2 Broekeart, J. A. C., *J. Anal. At. Spectrom.*, 1987, **2**, 537.
3 Bengston, A., *Spectrochim. Acta, Part B*, 1994, **49**, 411.
4 Winchester, M. R., Lazik, C., and Marcus, R. K., *Spectrochim. Acta, Part B*, 1991, **46**, 483.
5 Hutton, R. C., and Raith, A., *J. Anal. At. Spectrom.*, 1992, **7**, 623.
6 Tong, S. L., and Harrison, W. W., *Spectrochim. Acta, Part B*, 1993, **48**, 1237.
7 de Gendt, S., van Grieken, R., Hang, W., and Harrison, W. W., *J. Anal. At. Spectrom.*, 1995, **10**, 689.
8 Sanderson, N. E., Hall, E., Clark, J., Charalambous, P., and Hall, D., *Mikrochim. Acta*, 1987, **1**, 275.
9 Smithwick, R. W., III, Lynch, D. W., and Franklin, J. C., *J. Am. Soc. Mass Spectrom.*, 1993, **4**, 278.
10 King, F. L., and Harrison, W. W., *Mass Spectrom. Rev.*, , 1990, **9**, 285.
11 Feng, X., and Horlick, G., *J. Anal. At. Spectrom.*, 1994, **9**, 823.
12 U.S. Patent No. 4,853,539 to VG Instruments Group, Ltd., Hall, D. J., Sanderson, N. E., and Hall, E. F. H., Aug. 1, 1989.
13 Ohorodnik, S. K., and Harrison, W. W., *Anal. Chem.*, 1993, **65**, 2542.
14 Ratliff, P. H., and Harrison, W. W., *Spectrochim. Acta, Part B*, 1994, **49**, 1747.
15 Ohorodnik, S. K., DeGendt, S., Tong, S. L., and Harrison, W. W., *J. Anal. At. Spectrom.*, 1993, **8**, 859.
16 Greenwood, N. N., and Earnshaw, A., *Chemistry of the Elements*, 1st edn., Pergamon Press, Oxford, 1984, pp. 1335–1336.
17 Donohue, D. L., and Petek, M., *Anal. Chem.*, 1991, **63**, 740.
18 van Straaten, M., Swenters, K., Gijbels, R., Verlinden, J., and Adriaenssens, E., *J. Anal. At. Spectrom.*, 1994, **9**, 1389.
19 Smith, M. E., *Anal. Chim. Acta*, 1981, **130**, 215.
20 Bogaerts, A., Gijbels, R., and Goedheer, W. J., *J. Appl. Phys.*, 1995, **78**, 2233.
21 Bogaerts, A., van Straaten, M., and Gijbels, R., *J. Appl. Phys.*, 1995, **77**, 1868.
22 van Straaten, M., Gijbels, R., and Vertes, A., *Anal. Chem.*, 1992, **64**, 1855.
23 Mason, R. S., Milton, D. M. P., Pichilingi, M., Anderson, P. D. J., and Fernandez, M. T., *Rapid Commun. Mass Spectrom.*, 1994, **8**, 187.
24 Mei, Y., and Harrison, W. W., *Spectrochim. Acta, Part B*, 1991, **46**, 175.
25 Ortner, H. M., *Fresenius J. Anal. Chem.*, 1992, **343**, 695.
26 Takahashi, T., and Shimamura, T., *Anal. Chem.*, 1994, **66**, 3274.
27 Teng, J., Barshick, C. M., Duckworth, D. C., Morton, S. J., Smith, D. H., and King, F. L., *Appl. Spectrosc.*, 1995, **49**, 1361.
28 Jakubowski, N., Feldmann, I., and Stuewer, D., *Spectrochim. Acta, Part B*, 1995, **50**, 639.
29 Jones, D. G., Payling, R., Gower, S. A., and Boge, E. M., *J. Anal. At. Spectrom.*, 1994, **9**, 369.
30 Jakubowski, N., and Stuewer, D., *J. Anal. At. Spectrom.*, 1992, **7**, 951.

Paper 6/02169G
Received March 27, 1996
Accepted July 16, 1996